Journal of Materials Chemistry A

ROYAL SOCIETY OF CHEMISTRY

PAPER

View Article Online
View Journal | View Issue

Cite this: J. Mater. Chem. A, 2025, 13, 35435

Measuring the buried interphase between solid electrolytes and lithium metal using neutrons†

Andrew S. Westover, *[a] Katie L. Browning,[a] Antonino Cannavó,[b] Ralph Gilles,*[c] Jiri Vacik,[d] James F. Browning,[e] Neelima Paul,[c] Giovanni Ceccio[d] and Vasyl Lavrentiev[d]

Interfaces are the key to next-generation high-energy batteries including solid-state Li metal batteries. In solid-state batteries, the buried nature of solid–solid electrolyte–electrode interfaces makes studying them difficult. Neutrons have significant potential to non-destructively probe these buried solid–solid interfaces. This work presents a comparative study using both neutron depth profiling (NDP) and neutron reflectometry (NR) to study a model lithium metal–lithium phosphorus oxynitride (LiPON) solid electrolyte system. In the NDP data, no distinct interphase is observed at the interface. NR shows a difference between electrodeposited, and vapor deposited LiPON–Li interfaces but finds both are gradient interphases that are less than 30 nm thick. Additional simulations of the LiPON–Li_2O–Li system demonstrate that NDP has an excellent resolution in the 50 nm–1 μm regime while NR has an ideal resolution from 0.1–200 nm with different sample requirements. Together NDP and NR can provide a complementary understanding of interfaces between Li metal and solid electrolytes across relevant length scales.

Received 17th July 2025
Accepted 6th September 2025

DOI: 10.1039/d5ta05758b

rsc.li/materials-a

Andrew S. Westover

Andrew S. Westover is a staff scientist at Oak Ridge National Laboratory with a focus on solid-state batteries. Andrew obtained his PhD from Vanderbilt University in 2016 in interdisciplinary materials science and engineering. After graduating he worked at Oak Ridge National Laboratory as a postdoctoral research associate for 1 year before transitioning to a permanent staff position in 2018. In 2024, Andrew was awarded a prestigious ARPA-E IGNITE early career award. His research focuses on Li metal for solid-state batteries, the mechanics of solid-state batteries, using neutrons to probe battery interfaces, and the development of ductile bulk ionic glasses.

Introduction

The performance of high energy density batteries including solid state Li metal batteries is defined by the quality of the electrode–electrolyte interfaces.[1–3] Solid-state batteries using Li metal paired with solid electrolytes are one of the most promising electrode–electrolyte combinations for next generation batteries.[2,4–7] The nature of this cell design contains solid–solid electrode–electrolyte interfaces that are buried.[3,8,9] Developing methodologies that can enable the study of these buried solid–solid interfaces is critical for optimizing these solid-state Li metal batteries and realizing their potential. Neutrons have long been effective due to their non-destructive evaluation of materials.[3,10–18] For battery applications, neutron depth profiling (NDP),[12,14,15,19–21] neutron reflectometry (NR),[11,13,22–24] and neutron imaging (NI)[25–27] have been proposed to study the interfaces within batteries at various length scales. Each of these techniques have unique advantages and challenges that

[a]Chemical Sciences Division, Oak Ridge National Laboratory, Oak Ridge, 37830, USA. E-mail: westoveras@ornl.gov
[b]Collider Accelerator Department, Brookhaven National Laboratory, Upton, NY 11973, USA
[c]Heinz Maier-Leibnitz Zentrum, Technical University Munich, 85748, Garching, Germany. E-mail: ralph.gilles@frm2.tum.de
[d]Nuclear Physics Institute, Czech Academy of Sciences, CZ-25068, Rez, Czech Republic
[e]Neutron Scattering Division, Oak Ridge National Laboratory, Oak Ridge, 37830, USA

† This manuscript has been authored by UT-Battelle, LLC, under contract DE-AC05-00OR22725 with the US Department of Energy (DOE). The US Government retains and the publisher, by accepting the article for publication, acknowledges that the US government retains a nonexclusive, paid-up, irrevocable, worldwide license to publish or reproduce the published form of this manuscript or allow others to do so, for US government purposes. DOE will provide public access to these results of federally sponsored research in accordance with the DOE Public Access Plan (http://energy.gov/downloads/doe-public-access-plan).

will make them ideal for evaluating interfaces in different situations and materials systems.

The discovery of the solid electrolyte lithium phosphorus oxynitride (LiPON) in the 90's was instrumental in the field of solid-state batteries.[28–31] This electrolyte enabled the invention and commercialization of the thin film battery with a thin sputtered cathode such as $LiCoO_2$, a LiPON electrolyte and a Li metal anode.[31] These batteries have been cycled for >10 000 cycles[28,29] and have demonstrated charging current densities up to 10 mA cm^{-2}.[30] Because of the battery form factor and method of synthesis, the thin film geometry with LiPON and Li metal is an ideal model system to probe the Li/solid electrolyte interphases. Indeed, several studies have evaluated the interface between LiPON and Li metal and LiPON and cathodes.[3,8,32,33] Transmission electron microscopy (TEM) has been one of the most effective methods but is necessarily limited by difficult sample preparation such as cryogenic focused ion beam (Cryo-FIB), which may alter the interfaces.[32,33] TEM is also limited to small sample volumes that may or may not represent real life battery interfaces which can range in areal footprint from cm to m. Electroanalytical techniques have also been used to demonstrate LiPON's ability to effectively passivate Li metal anodes through formation of a less than 10 nm thick interphase.[8] These techniques are themselves limited by the indirect nature of the methods and work best in conjunction with TEM or neutron techniques. NR has also been used coupled with Coulombic titration to evaluate the interface of LiPON with Li metal confirming that on average the interphase between LiPON and Li metal is less than 10 nm thick.[3]

In this work, we build on prior NR studies[3] and compare NDP and NR datasets to identify advantages and limitations of each technique. The NDP data shows a detailed profile of the LiPON/Li metal sample stack. Model fits to the NDP data show no difference between models with and without an interphase layer, highlighting that NDP is unable to distinguish 10 nm thick interphase layers in these samples. When a 50 nm Ni layer is included in between the LiPON and Li, the 50 nm Ni layer is clearly distinguished in both the NDP data and the fitted model. Further simulations show that high Li content materials such as Li_2O need around 100 nm of interphase material to see the difference in the NDP data. To complement this data, NR was also performed on a similar Li/LiPON cell stack. In this case the NR resolves both an electrodeposited Li/LiPON gradient interphase less than 10 nm thick and a vapor deposited Li/LiPON interphase that is ~30 nm thick. Further modeling data shows that the NR is very sensitive for interphase layers between 10–200 nm thick. NDP on the other hand can handle thicker samples with generally less stringent sample requirements. Together this experimental and simulated data highlights the complimentary nature of both NDP and NR for studying interfaces in SSB. It should be emphasized that both methods gained an average result over many tens of mm^2 of sample size together with a deep penetration depth in the sample in comparison to classical microscopy methods.

Results and discussion

Fig. 1 shows a schematic of both NDP and NR for evaluating the interfaces between solid electrolytes and Li metal. In NDP thermal neutrons (energy of about 0.025 eV) are focused on a sample. The neutrons will react with ^{6}Li in the sample emitting both α and Triton radiation.[12,19,34,35] The α and Triton particles are emitted from the point of origin and lose energy in passing through the sample. More energy is lost the deeper the reaction occurs in the sample. By detecting the energy and quantity of the emitted radiation it is possible to identify the ^{6}Li concentration as a function of depth at which the particles were produced, allowing the construction of a Li-depth profile. This depth profile is measured as a distribution of counts per energy channel. For the purposes of this paper, the x-axis representing the probed depth is presented in energy units. NR measures the probability of a neutron of a given momentum to reflect off the surface of a sample.[36,37] Elastic neutron scattering of a cold neutron beam (energy from 5×10^{-5} eV to 0.025 eV) at small angles (typically smaller than a few degrees) to the sample surface leads to reflected neutrons with an intensity profile as a function of momentum transfer (Q) and angle dependence which can be interpreted as variations of the chemical composition or density of the film as a function of depth. The change in composition as a function of depth gives rise to interference patterns (measured as reflectivity curves) as the scattered wave of the neutrons acquires a different phase for each path through the thickness of the film. The sum of the coherent scattering lengths for each isotope of each atom per unit volume obtains the average scattering length density (SLD) as a measure of the scattering power of a material. Analysis of the Kiessig fringes in the reflectivity curve provides information on layer thickness, density, roughness, and composition.

The samples used in both the NDP and NR measurements were made using sputtering and thermal evaporation as detailed in Table 1 and Fig. S1. The sample sets for NDP contain both thin (~100 nm) and thick (~500 nm) LiPON films deposited on Li metal. Fig. 2 shows the α radiation NDP data for both thin and thick LiPON films deposited onto Li metal and onto the bare substrates as controls. NDP data is taken by measuring the intensity of the radiation emitted from the sample as a function of energy. The measured intensity indicates the number α particles of a given energy hitting the detectors. The Li concentration throughout the sample is then determined by analyzing the energy and count of the α particles. The goal of this set of measurements is to (1) determine if we can resolve a distinct interphase between Li and LiPON, (2) determine the estimated thickness of the interphase, and (3) determine the resolution of NDP for distinguishing interphases between Li metal and LiPON. For all 6 NDP samples we see a distinct high intensity peak coming from the Li metal and a lower intensity shoulder coming from the LiPON. In the next several paragraphs we will analyze the intensity and energy of the Li peak and the LiPON shoulder to answer the above questions.

Fig. 2a shows the NDP profile from the α radiation for the thin LiPON–Li sample (black) and the accompanying thin LiPON control (blue). For this thin LiPON–Li sample there is only a single peak centered at channel 2026 eV. The profile for the control (blue) shows that the LiPON peak is centered at 2050 eV and is convoluted within the Li peak. Simulation of the data (red circles in Fig. 2a and c) estimates the LiPON layer is

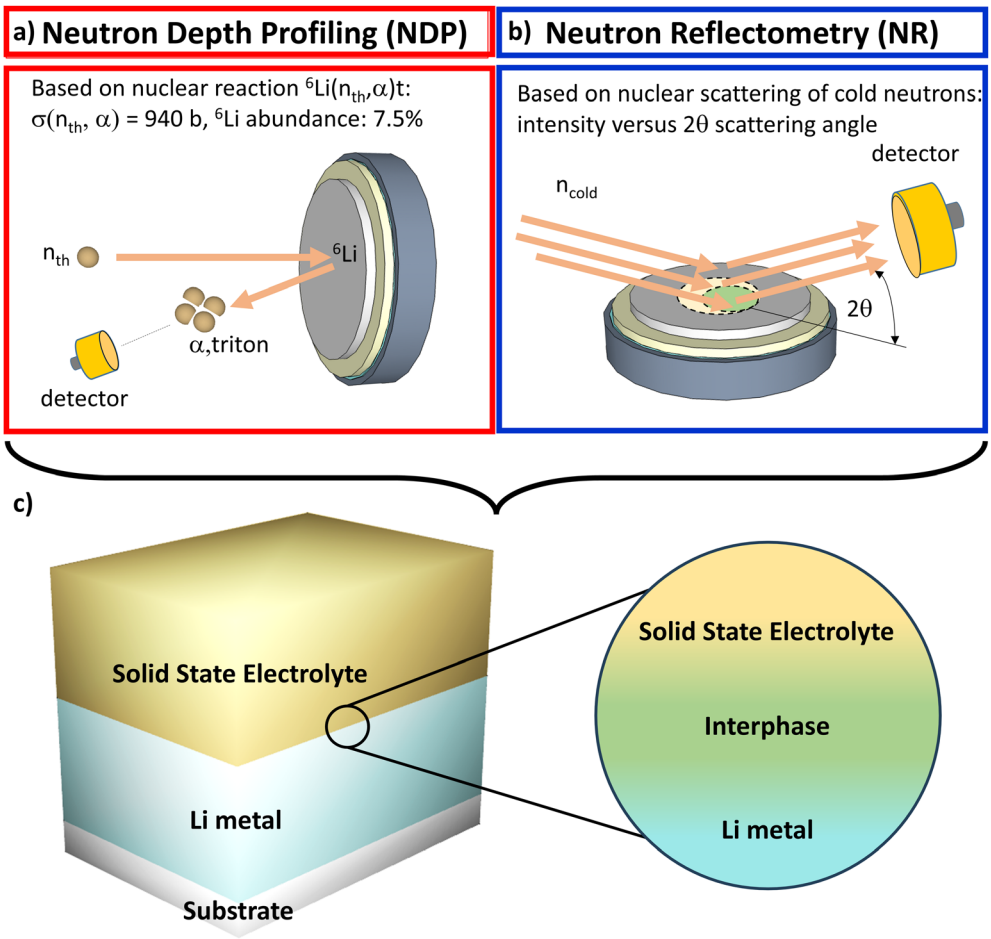

Fig. 1 a) Schematic illustration of neutron depth profiling (NDP) where thermal neutrons (n_{th}) penetrate a sample and react with ^{6}Li producing both α and Triton radiation which are then measured. (b) Schematic illustration of neutron reflectometry (NR) where cold neutrons (n_{cold}) reflect and refract through a thin film multilayer forming a reflected neutron spectra with both constructive and destructive interference resulting in a Kiessig fringe pattern on the detector. (c) Schematic illustration of a typical sample consisting of a solid electrolyte connected (SSE) paired with a Li metal electrode. The blowout highlights the formation of an interphase between the solid electrolyte and the Li metal which can be studied with both NDP and NR.

Table 1 Summary of the samples used for NDP and NR measurements

	Title	Layer 1	Layer 2	Layer 3
NDP-1	Thin LiPON	LiPON ∼100 nm		
NDP-2	Thin LiPON–Li	Li ∼500 nm	LiPON ∼100 nm	
NDP-3	Thin LiPON–Ni–Li	Li ∼500 nm	Ni ∼50 nm	LiPON ∼100 nm
NDP-4	Thick LiPON	LiPON ∼500 nm		
NDP-5	Thick LiPON–Li	Li ∼500 nm	LiPON ∼500 nm	
NDP-6	Thick LiPON–Ni–Li	Li ∼500 nm	Ni ∼50 nm	LiPON ∼500 nm
NR-1	LiPON–Li (NR)	Ni ∼10 nm	LiPON ∼200 nm	Li ∼2000 nm

77 nm thick, and the Li layer is 428 nm thick. Fig. 2c shows the NDP dataset for the Li coated with the thick LiPON (black) and the associated LiPON control (blue). In this case the Li peak center is shifted from 2026 eV down to 1956 eV. A LiPON shoulder is also clearly visible from 2002–2096 eV. The peak intensity for the LiPON shoulder is ∼3.4 times smaller than the Li peak as one would expect for the relative difference in Li concentration in Li metal *vs.* LiPON. The modeling data presented as the open circles fit in Fig. 2c and d shows a LiPON thickness of 294 nm and a Li thickness of 428 nm. The LiPON composition was assumed to be $Li_{2.94}PO_{3.50}N_{0.31}$ determined for LiPON deposited from the same process in the same deposition chamber.[38] In both cases there is also some Li that migrates into the Al_2O_3 substrate.[39] In the case of the thicker LiPON there appears to be a bit more Li that intercalates into the Al_2O_3. This could come from the generally larger Li content available or

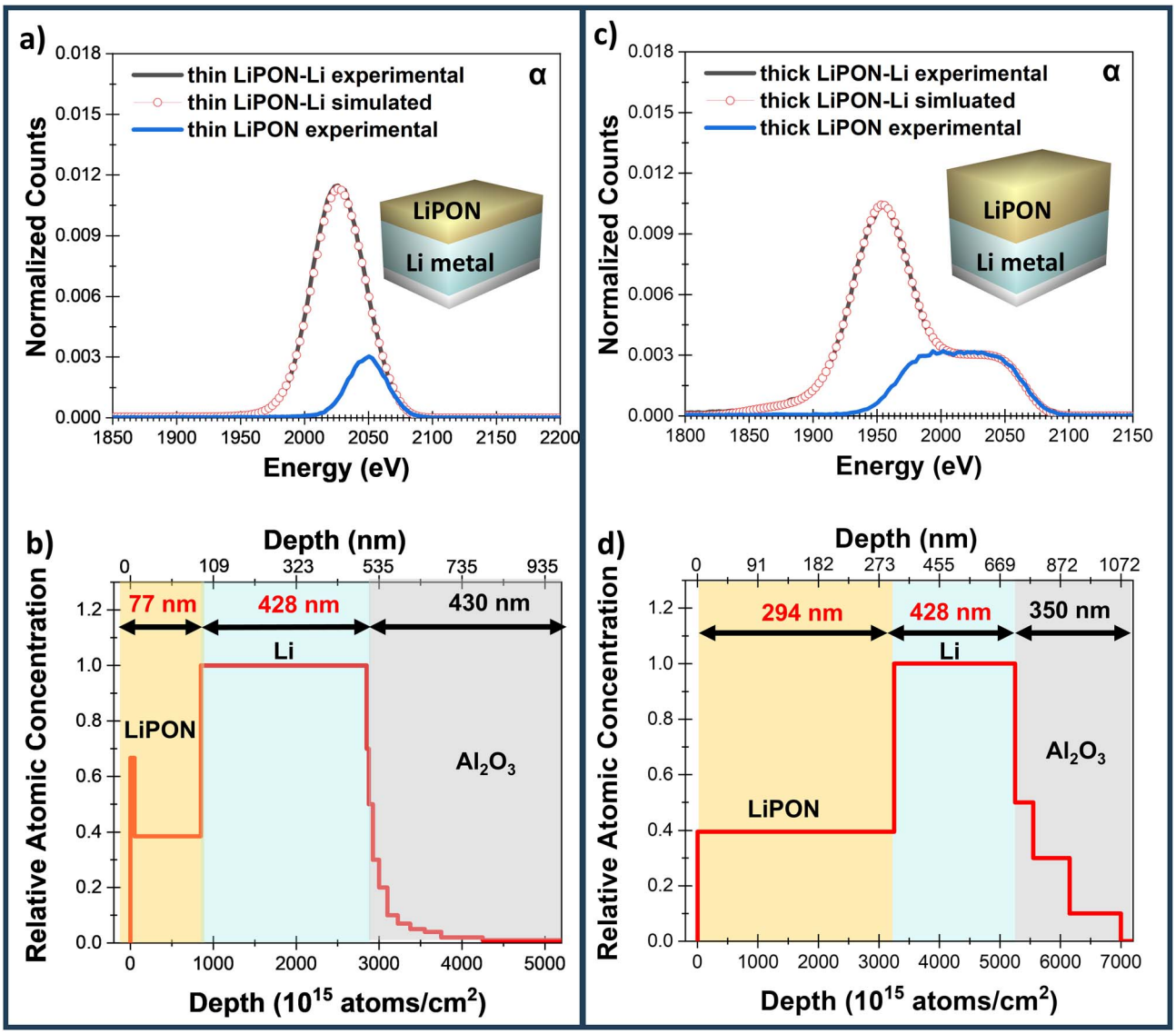

Fig. 2 (a) α radiation signal from neutron depth profiling of a sample consisting of nominally 100 nm of LiPON deposited onto 400 nm of Li metal. The black solid line shows the experimental data, and the red circles represent and simulated fit to the experimental data. The blue curve is the signal from a witness sample that only contained the 100 nm of LiPON. (b) A depth representation of the simulated data in a) showing an estimated LiPON thickness of 77 nm, and a Li thickness of 428 nm. (c) α radiation signal from neutron depth profiling of a sample consisting of 294 nm of LiPON deposited onto 428 nm of Li metal. The black solid line shows the experimental data, and the red circles represent and simulated fit to the experimental data. The blue curve is the signal from a witness sample that only contained the 294 nm of LiPON. (d) A depth representation of the simulated data in (b) showing a LiPON thickness of 294 nm and a Li thickness of 428 nm.

more likely from an increased temperature that arises on the substrate due to the longer sputtering time required for the thicker LiPON. In either case, the Li in the Al_2O_3 does not significantly impact the discussion on the LiPON–Li interface that is of primary interest in this work. A summary of the NDP energy ranges and intensities is provided in Table 2.

Based on this NDP data we can draw several key conclusions. First, for LiPON and the Li metal to be distinguishable the solid electrolyte needs to be at least 100–200 nm thick. Second, for this data there is no distinct interphase that is observed in the NDP data as demonstrated by the simulated data which contains no interphase, but shows an excellent fit to the LiPON data. As the interphase that forms between LiPON and Li metal is not easily distinguishable in NDP, the natural question is what is the resolution for measuring Li/SSE interphases with NDP? Included in the answer to that question is an upper bound for the interphase that forms between LiPON and Li metal.

To determine the spatial resolution of the NDP measurements we developed another set of samples with an artificial Ni based interphase between the Li metal and the LiPON. Due to the need for an air-free transfer the system used to deposit Ni was only equipped with RF magnetron sputtering with slow deposition rates. This resulted in some amount of O being

Table 2 Summary of energy ranges, peak positions, and peak intensitie for NDP measurements

	Sample description	Energy spread (eV)	Li peak center (eV)	Peak intensity (a.u.)	LiPON shoulder (eV)	LiPON shoulder intensity (a.u.)
NDP-1	Thin LiPON	2015–2096	—	—	2015–2096	0.0030
NDP-2	Thin LiPON–Li	1961–2096	2026	0.0113	—	—
NDP-3	Thin LiPON–Ni–Li	1907–2096	1980	0.0087	2015–2096	0.0031
NDP-4	Thick LiPON	1934–2096	—	—	1934–2096	0.0031
NDP-5	Thick LiPON–Li	1880–2096	1956	0.0105	2001–2096	0.0031
NDP-6	Thick LiPON–Ni–Li	1853–2096	1910	0.0083	1947–2096	0.0030

included in the films enabling some Li from the LiPON deposition to react with the NiO layer forming a mixed Li–Ni–O layer. For simplicity, the labeling just uses Ni. Fig. 3 shows the NDP results for both the thin LiPON–Ni–Li and thick LiPON–Ni–Li layers. For the sample with the thin LiPON layer, the Ni shifted the Li peak center to lower energy from 2026 eV (Fig. 2a, Ni-free sample) to 1980 eV (Fig. 3a, Ni-based sample). This had two distinct benefits, first the LiPON shoulder from 2015–2096 eV

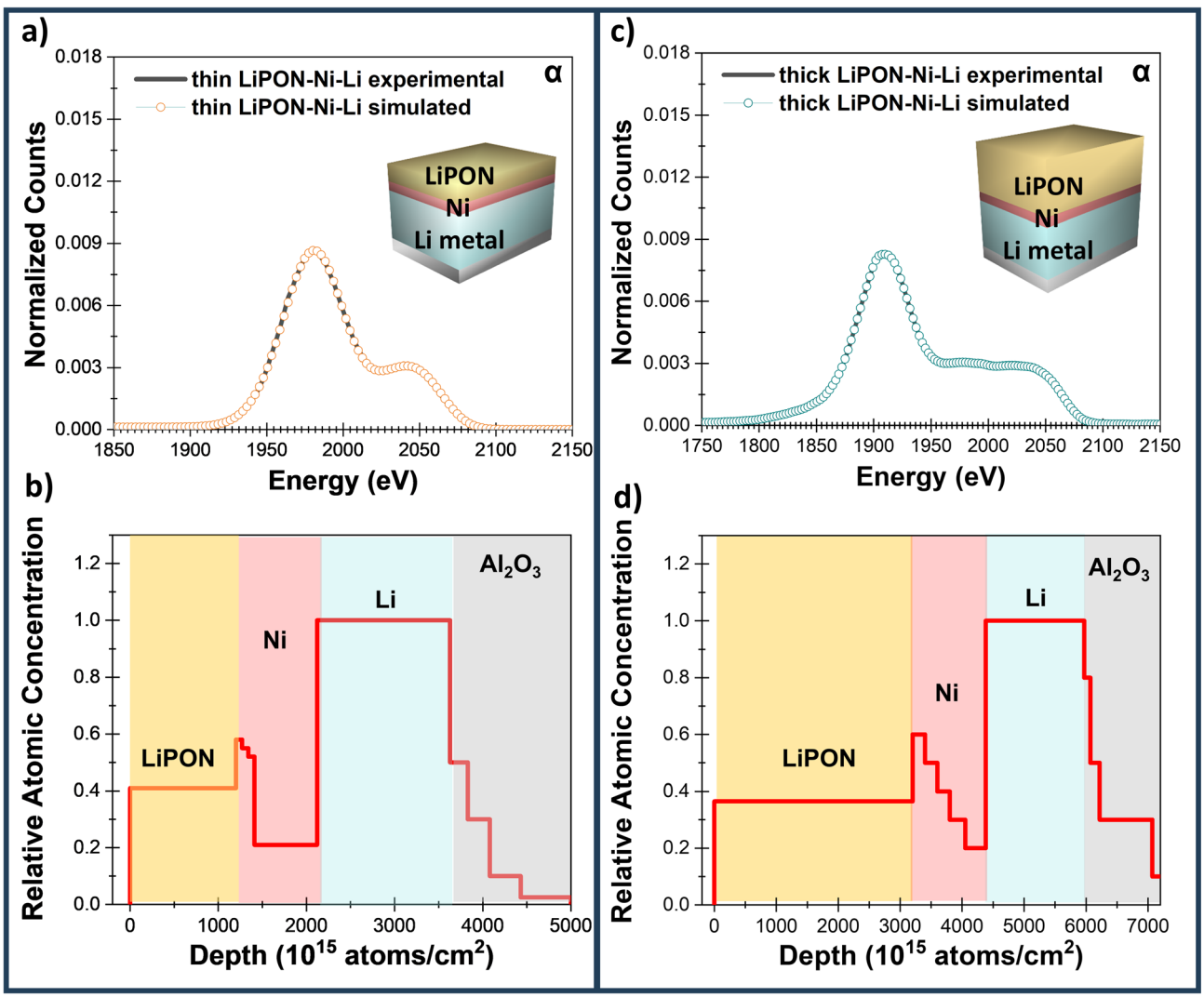

Fig. 3 (a) α radiation signal from neutron depth profiling of a sample consisting of nominally 100 nm of LiPON deposited onto ~50 nm of Ni and 400 nm of Li metal. The black solid line shows the experimental data, and the orange circles represent and simulated fit to the experimental data. (b) A depth representation of the simulated data in a) represented in terms of atoms per cm^{-2} due to uncertainty in the Ni density. (c) α radiation signal from neutron depth profiling of a sample consisting of nominally 300 nm of LiPON deposited onto 50 nm of Ni and 400 nm of Li metal. The black solid line shows the experimental data, and the red circles represent and simulated fit to the experimental data. (d) A depth representation of the simulated data in (b) represented in terms of atoms per cm^{-2} due to uncertainty in the Ni density.

becomes distinct from the Li peak. Second there is a clear dip in the α particle intensity between the LiPON and Li peaks indicating a Li poor NiO region. Because of the uncertainty in the density and exact composition of the NiO interlayer, the thickness could not be estimated, but a model with a good fit was also produced using an estimate for the # of atoms per cm^{-2} clearly showing this distinct Ni rich interphase layer (Fig. 3b). Atoms per cm^{-2} are units commonly used in interpreting NDP data. This unit is based on the depth (cm)* atomic density $\left(\frac{\text{atoms}}{\text{cm}^3}\right)$ to yield units of atoms per cm^{-2}. This model clearly shows a LiPON layer that extends from 0–1.20 $\times$ 10^{18} Li atoms per cm^{-2}, a Ni based interlayer that goes from 1.20–2.12 $\times$ 10^{18} Li atoms per cm^{-2}, and finally a Li layer that extends from 2.12–3.63 $\times$ 10^{18} Li atoms per cm^{-2}. Based on the Quartz Crystal Microbalance (QCM) from the deposition, the Ni layer is approximately 50 nm thick. For the thick LiPON–Ni–Li sample presented in Fig. 3c, the Li peak center also shifts to lower energy from 1956 eV (Figure 2c) to 1910 eV (Fig. 3c). The Li peak intensity also decreases from 0.0105 to 0.0083. This occurs due to Li migration into the NiO layer. Similarly, the model fitted to the experimental data shows the thicker LiPON layer extending from 0–3.20 $\times$ 10^{18} atoms per cm^{-2}, followed by the Li rich NiO layer from 3.20–4.38 $\times$ 10^{18} atoms per cm^{-2}, and finally Li layer from 4.38–5.97 $\times$ 10^{18} atoms per cm^{-2}. One difference between the Ni layer in the thick *vs.* thin LiPON films is the degree of lithiation. More Li migrates into the Ni layer during the synthesis of the thicker LiPON film. Similar to the increased Li in the Al_2O_3 layer, this likely occurs due to the increased temperature during deposition of the thicker LiPON film, or an *in situ* lithiation effect that can occur during sputtering.[40]

Based on this data, the more subtle natural interphase between LiPON and Li metal is difficult to detect, but the higher

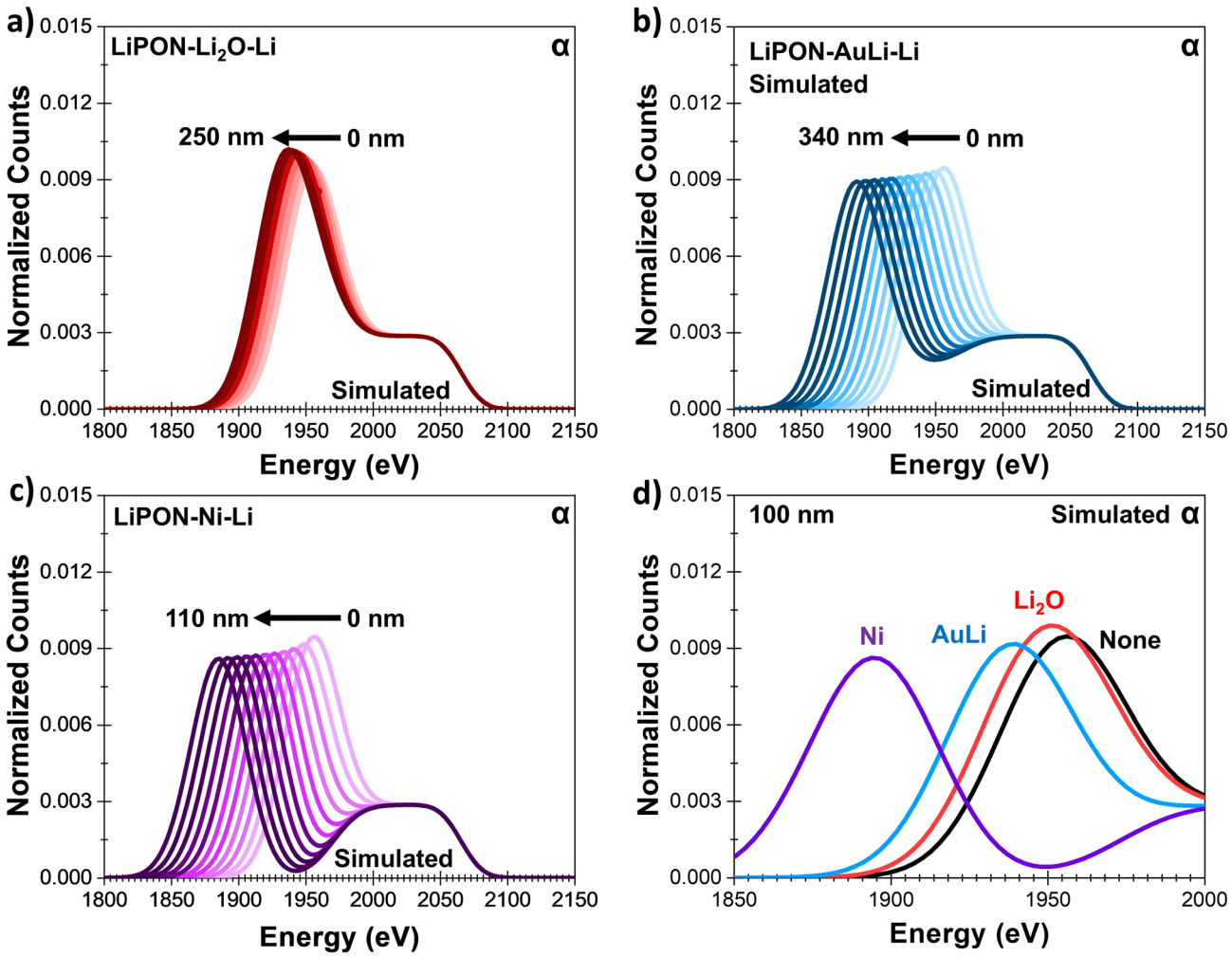

Fig. 4 (a) Simulated neutron depth profile showing the alpha radiation signal for a LiPON/Li system with a simulated Li_2O interphase layer ranging in thickness from 0 to 250 nm. (b) Simulated neutron depth profile showing the alpha radiation signal for a LiPON/Li system with a simulated AuLi alloy interphase layer ranging in thickness from 0 to 340 nm. (c) Simulated neutron depth profile showing the alpha radiation signal for a LiPON/Li system with a simulated Ni metal interphase layer ranging in thickness from 0 to 110 nm. (d) simulated NDP profiles focused on the Li metal peak comparing the impact of 100 nm interlayers of Li_2O, AuLi, and Ni metal. All the spectra here show simulated results for α radiation. For the figures the interlayers were considered to be stoichiometric crystalline Li_2O (2.01 g cm^{-3}), AuLi (10.49 g cm^{-3}), and Ni metal (8.90 g cm^{-3}).

atomic number (Z) of the Ni based interphase is more easily distinguished. To better understand the resolution limits for different types of interphase layers between Li metal and SSE we performed a series of simulations. In these simulated NDP data we used the thick LiPON–Li metal samples as a baseline and artificially inserted interphase layers of different composition and thicknesses ranging from 0–1000 $\times$ 10^{15} atoms per cm^{-2} in 100 $\times$ 10^{15} atoms per cm^{-2} increments. The exact thickness of each layer is material dependent due to differences in density. We did this with three different interphase materials: Li_2O which is the most likely byproduct of natural interphase layers with oxide electrolytes, a AuLi alloy layer representing one of the most compelling strategies for interphase stabilization,[41,42] and a Ni interphase representing a nominally completely Li free interphase layer. As each of these materials have different densities and molar masses, this leads to interphase thicknesses of 0–250 nm for Li_2O, 0–340 nm for the AuLi alloy, and 0–110 nm for Ni metal. These cases represent some of the most interesting interlayer approaches to enable solid-state batteries. Fig. 4a and S3 shows the effect of the Li_2O layers with different thicknesses 0 nm-250 nm. As the Li_2O interlayer thickness increases, the Li metal peak center shifts to lower energy from 1956 eV with no interphase to 1937 eV with the thickest 250 nm Li_2O layer. For the AuLi alloy interlayer (Fig. 4b), the central Li peak has a much more dramatic shift to lower energy from 1956 eV down to 1888 eV at 350 nm. A distinct dip in the intensity of the NDP profile is also observable starting with thicknesses of ~100 nm. For the Li-free Ni metal interlayer data (Fig. 4c) we see a downshift in the Li peak center from 1956 eV to 1883 eV at 110 nm. The distinct dip in the data also happens more quickly with thicknesses starting at 21 nm. To show a more direct comparison Fig. 4d shows the three interlayer types with thicknesses of ~100 nm compared to the Li peak with no interlayer. At 100 nm all three types of interphases are distinguishable as a shift of the Li peak to lower energy with shifts from 1956 eV with no interphase to 1951 eV, 1940 eV, and 1893 eV for Li_2O, LiAu, and Ni respectively. Based on these simulations NDP is unlikely to be able to resolve interphase layers <100 nm thick for the low Z compounds or ~10 nm for layers with higher Z as can be seen with the Ni and Au based layers. The reason for this, is that while the NDP only detects the Li, the energy loss for the emitted radiation is larger when passing through higher Z based compounds.

While the discussion here has focused on α radiation as this is more depth sensitive, triton radiation is also produced when the neutrons penetrate through the sample. The experimental triton radiation datasets for the thin LiPON–Li and thick LiPON–Li as well as the simulated Li_2O and Ni interlayer series is presented in Fig. S4. In all these datasets there is a single Li peak centered at 2717 eV. The thicker LiPON shifts this slightly to 2712 eV. The Li_2O series and the Ni series also do not cause a distinct layer separation but result in peak shifts to 2709 eV and 2698 eV, respectively. Because the triton radiation is less sensitive to minor changes that would occur due to an interphase, it is not the focus of this work. The advantage to triton radiation is that the triton radiation can cover a larger energy range accommodating the measurement of thicker samples.[12]

Before considering NR, there is one other important factor for NDP to discuss. When measuring an artificial interphase such as the Ni layer presented in Fig. 3, NDP shows a distinct peak shift. But in many cases the interphase of most interest is the natural interphase between a solid electrolyte and Li metal or a cathode. This interphase occurs when the solid electrolyte is contacted with the electrode and typically occurs spontaneously or after the first few electrochemical cycles. For these natural interphases there will be a change in chemistry, but the total number of atoms will not change. Thus, the location of the Li peak will not shift down as we see with the artificial interphases in Fig. 4. Rather, these naturally occurring interphases will primarily be visible as a decrease in the intensity of the Li peak coupled with a broadening of the peak as some of the Li migrates into the solid electrolytes. The lithiation of the Ni layer in Fig. 3 is an excellent example of what we would expect to see when the reaction between the solid electrolyte and Li metal are more prevalent than the reaction of Li with LiPON. One way to enhance the visibility of this effect would be to use isotopes. For example, if the Li metal anode was composed entirely of ^{6}Li and the electrolyte of ^{7}Li then the reaction of ^{6}Li with the electrolyte would be significantly more visible than with naturally occurring Li like that used in this study.

Previously we performed an *in situ* NR measurement of the interphase formation between LiPON and Li metal.[3] This experiment consisted of a quartz substrate with 10 nm of Ni, 200 nm of LiPON and 2 μm of Li where Li was plated onto the Ni through the LiPON. After an interphase had formed, Li was subsequently stripped, and the reflectivity measurement was performed. From this data, a gradient Li–LiPON interphase of 7 nm was identified. Building on that work here we used a similar sample stack with 200 nm of LiPON and 2 μm of Li on a Ni coated quartz substrate as a baseline to explore the sensitivity of NR to interphases of different thicknesses and to probe some of the limits of the technique in comparison to NDP. More details of the synthesis can be found in the SI. Fig. 5 shows the reflectivity pattern from the NR measurement. Q in these measurements is the neutron scattering vector. A fit to the data is shown in black in Fig. 5a. The scattering length density (SLD) plot associated with this fit is shown in Fig. 5b. The data shows an initial Ni layer that was on the quartz substrate followed by a thin Li layer (6.5 nm), a LiPON layer (206 nm), and a thick semi-infinite Li layer greater than 1 μm. The Ni was deposited on the substrate for possible *in situ* measurements, but the sample was not used for that purpose (details in the SI). The thin Li layer deposited on the Ni comes from a battery-like lithiation effect that can occur during the magnetron sputtering of LiPON. During sputtering, the plasma causes a bias that builds up across the LiPON electrolyte that is being deposited. The plasma also acts as a current path creating a battery like effect where Li can transport through the LiPON and either deposit Li or lithiate a cathode underneath the freshly deposited LiPON (see reference for more details).[40] With two distinct Li layers on either side of the LiPON we have the opportunity to use NR to compare the interphase that forms at the inner electrodeposited Li/LiPON interface and the outer vapor deposited LiPON/Li interface. For the inner electrodeposited Li/

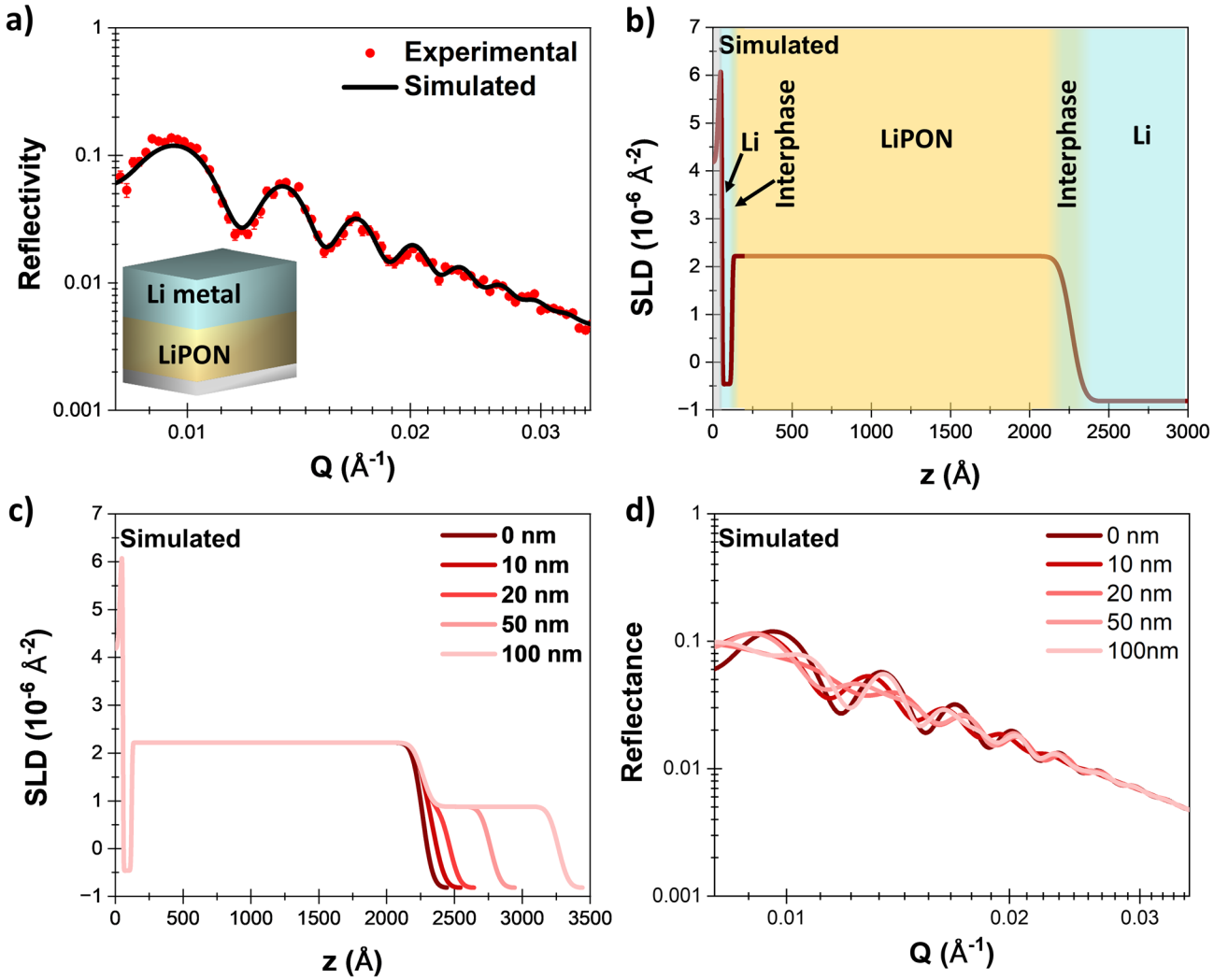

Fig. 5 (a) NR spectra shown with the reflectivity intensity for a 200 nm LiPON sample with several microns of Li metal deposited on top. The red dots are the experimental data, and the black line is the simulated fit to the experimental data. (b) scattering length density (SLD) of the simulated fit to the experimental data in (a) as a function of depth with the LiPON layer represented in yellow, the Li metal represented in blue, and the interphase represented in green. (c) SLD as a function of depth for a simulated sample stack based on the experimental stack in (a) but with an additional artificial Li_2O interphase layer included between the Li and LiPON layers with thicknesses of 0, 10, 20, 50 and 100 nm. (d) Simulated Kiesseg fringes for the sample series in (c).

LiPON interphase, we observe a gradient interphase that extends from a depth of 10 nm to a depth of 14 nm for a total interphase of ~4 nm. This truly highlights the power NR in precisely measuring thin interphase layers. While this inner interphase is very thin, the outer interphase between the LiPON and the vapor deposited Li extends from 208 nm to 243 nm for a total thickness of 36 nm. The discrepancy between this thinner inner Li/LiPON interphase and the outer LiPON–Li interphase likely comes from a rougher outer LiPON surface that can occur during sputtering of ceramics and glasses. Indeed, atomic force microscopy (AFM) data for the control LiPON films deposited for NDP shows a roughness on the order of 10 nm (Fig. S5). For the films with LiPON and Li metal the AFM data shows a roughness of 20–50 nm. Because of the convolution with the roughness, the true chemical interphase that arises from the reaction of LiPON with Li metal is more accurately reflected by the sharp inner interphase layer. This data also matches well with the prior *in situ* measurement of the interphase with NR and a similar *in situ* measurement using Coulombic titration.

To understand the limitations of NR in the context of a solid electrolyte and Li metal, we performed a series of simulations modifying the fit to the experimental dataset in Fig. 5a with distinct Li_2O interlayers added in between the outer LiPON and Li layers. This data is shown in Fig. 5c–d. Fig. 5c shows the simulated SLD patterns for Li_2O thicknesses of 10, 20, 50, and 100 nm. The corresponding simulated reflectivity data are shown in Fig. 5d. This data highlights significant changes in the Kiessig fringes across the Q spectrum shown. The data shows that NR effectively captures interphase layers less than 100 nm. While the focus of this work is on interphase layers, it also highlights some of the challenges that NR faces in terms of the

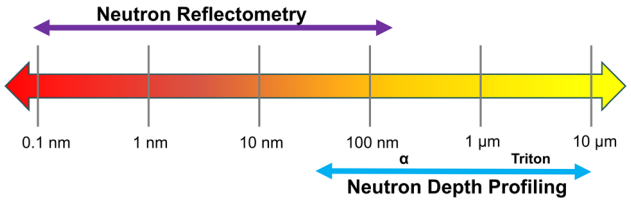

Fig. 6 Schematic of the relative sensitivity ranges for neutron reflectometry and neutron depth profiling.

needed sample geometry where the thin layers of interest must be less than ~400 nm thick. The roughness of the substrate or solid electrolyte layers will also convolute the interpretation of the data.

From the combined NDP and NR datasets and modeling it is clear both techniques have advantages and disadvantages that can be grouped into three categories: (1) length scale resolution (Fig. 6), (2) sample requirements, and (3) chemical sensitivity (Table 3). Regarding length scale resolution, NR is most effective for detecting thin interphase layers, but NDP may be better suited for thicker interphase greater than 100 nm. For NR, the roughness of the sample is the primary limitation. Practically speaking for very smooth surfaces the resolution limit is on the order of a few nanometers. For thicker interphases, NR has some significant limitations as film stacks need to be less than ~400 nm for high-quality data. In this work, we showed how a thin electrolyte film sputtered onto one of these substrates enables probing of the interphase between that solid electrolyte and Li metal. Another potential approach for ceramic or glass electrolytes includes using thick, highly polished electrolyte substrates on the order of the dimensions of the traditional NR substrates ~2″ diameter and $\frac{1}{4}$″ thick. Li metal could then be applied to these electrolytes by vapor deposition or melt casting. If the interphase was then less than 400 nm thick it could be resolved with NR. Another limitation of NR is that the chemical sensitivity of the technique primarily lies in the fitted values of SLD to the NR pattern. While the SLD of something like Li metal (−0.89) is relatively unique compared to almost all other compounds, the SLD of the different electrolytes and interphase layers could be similar convoluting the data and making it difficult to pinpoint exact chemical compositions. This is especially true as the SLD is also dependent on the density of the material. If the material in question is not fully dense then the SLD will be different.

For NDP, the length scale at which it excels is between 50 nm and 10 μm (Fig. 6). The length scale resolution is also heavily dependent on whether α or Triton particles are being used to determine the thickness of the interphase. For α particles, the resolution of the interphases is roughly between a few tens of nm and 5 μm. This lower limit is especially true for very thin samples. For NDP a low roughness is ideal. When using α particles, the biggest limitation is that the total sample thickness needs to be less than 10 μm. If it is not, then the α and Triton signals begin to overlap convoluting the sample. Triton particles on the other hand are less sensitive to very small thicknesses (Fig. S4) but can be used to study films tens of microns thick when Kapton or another material is used to block the α particles. From a chemical sensitivity standpoint, NDP is specifically sensitive to Li content. This limits some broader applications such as for Na applications (here radioactive ^{22}Na is necessary for high detection sensitivity) but also makes the technique especially useful for Li containing samples. NDP is most powerful when significantly different quantities of Li are contained in the different layers of interest.

While not the focus of this paper, neutron imaging (NI) is a third technique for studying interfaces in solid-state batteries. NI is in the tomography family of techniques which enables more direct imaging of a sample. Because the minimum resolution of NI is on the order of 1 to 2 μm it is not suitable for measuring interphase between solid electrolytes and Li metal or cathodes. NI can probe length scales on the order of 10 μm up to a few cm. This enables one to image an entire full cell battery stack which is not feasible with NR and NDP. Thus, NI is very well suited to observe the micron length scale morphological evolution of the interface during battery cycling.[44]

While in this publication we have focused on a model LiPON–Li SSE system, it is important to consider the broader applicability of this technique to other materials. This is especially the case when considering the most common electrolytes are sulfides such as Li_3PS_4 and the argyrodite Li_6PS_5Cl, and the oxide $Li_7La_3Zr_2O_{10}$ (LLZO). Both of these electrolyte classes have been observed using NDP as seen in the work by Han *et al.*[12] In this publication the authors were trying to understand the impact of electronic conductivity on internal deposition of Li metal. Notably, for the oxide LLZO and the sulfide Li_3PS_4 studied, they used very thick samples. To enable study by NDP, Kapton tape was used to block the alpha particles and Triton particles were used to measure the depth profile. In these measurements they could not profile the entire electrolyte–Li system due to the thickness, but they could focus on the interface. In these measurements the roughness of the samples prevented a precise study of the interface between the Li and the SSE. To use NDP to study the interphase between these SSE

Table 3 Comparison of key parameters used for NDP and NR

	NDP	NR
Interfacial resolution	α – >50 nm, triton – >100 nm	0.1–300 nm
Roughness requirement	<50 nm	< 1 nm
Maximum sample thickness	α – ~5 μm, triton – 30 μm	500 nm (area of interest)
Chemical sensitivity[43]	^{3}He, ^{6}Li, ^{14}N, ^{10}B	Broad, but dependent on SLD
Typicals sample size	1 cm^2	~20 cm^2

systems some careful adjustments will be required. The first is to minimize the roughness. The most conceptually straightforward path would be to sputter the different electrolytes as done with LiPON in this system. That said, developing pellets that are then polished down to nm scale roughness should also enable the study of the interfaces with both NDP and NR. While this may be a bit more difficult with sulfides, with LLZO or other oxide systems there has been impressive work in developing single crystal electrolytes that are completely transparent indicative of a very fine surface finish.[45] Li metal could then be melted or evaporated onto the electrolyte to enable study by NDP and NR. So while a bit more difficult than LiPON, it should be viable to study other SSE interfaces with these techniques. Going forward, of particular interest is to observe the change in the interfaces as cells are cycled. While initial *in situ* work has been done on the LiPON–Li system with NR,[3] other electrolyte systems such as the sulfides that are plagued with more significant interfacial challenges would benefit greatly from interfacial studies using NR and NDP.[46] We would expect the interfaces to be significantly thicker in these systems and should thus be readily observable. The oxide systems in most cases seems to have a similar ability with Li metal as LiPON and would likely need NR to resolve the interfaces. Some doped versions of LLZO and other oxides however also have reactivity challenges with Li metal which would also benefit from *in situ* electrochemical NDP and NR studies.[47]

Conclusions

In conclusion, we have compared the use of NDP and NR to study the interphase between Li metal and the solid electrolyte LiPON both with experimental and simulated data. Both techniques confirm LiPON and Li metal form a nm thin interphase layer, with NDP demonstrating it is less than ∼100 nm thick and NR measuring a gradient interphase ∼4 nm thick between electrodeposited Li and LiPON and a gradient interphase <35 nm thick between vapor deposited Li metal and LiPON. This comparative study clearly demonstrates both the power and limitations of both NDP and NR for studying interphases in solid state batteries. NR has significantly higher resolution allowing one to measure interphase thicknesses down to the nm length scale but is less effective at measuring thicker interphase layers. NR also comes with very stringent sample preparation requirements in terms of sample roughness and total interphase thickness. NDP on the other hand has a limited lower limit to the resolution but can measure thicker interphases. NDP samples are also not as limited by the sample roughness and the total sample thickness can be 10s of μm. Both techniques have great promise to be powerful tools in understanding the buried solid–solid interfaces in solid state batteries.

Author contributions

The manuscript was written through the contributions of all authors. All authors have approved the final version of the manuscript.

Conflicts of interest

There are no conflicts of interest to declare.

Data availability

The data associated with this manuscript is included as a SI excel file sorted by figure number. Supplementary information: Experimental methods, visual schematic and photographs of samples, triton radiation NDP data, atomic force microscopy of NDP samples. See DOI: **https://doi.org/10.1039/d5ta05758b**.

Acknowledgements

The work was funded by the Department of Energy's Office of Energy Efficiency and Renewable Energy for the Vehicle Technologies Office's US-German Cooperation on Energy Storage: Lithium–Solid–Electrolyte Interfaces program. R. G. and N. P were funded by the Federal Ministry of Education and Research (BMBF) under grant number 03XP0509C. Funding for the NDP portion of the work was also supported by the Ministry of Education, Youth and Sports (MŠMT) of the Czech Republic within the project CZ.02.01.01/00/22_008/0004591. The authors would like to thanks Mathieu Doucet for significant contributions in performing the neutron reflectometry experiments and for performing the additional simulations of artificial interface layers for the NR data presented in Fig. 5. The authors would like to acknowledge, Tien Duong, the US program manager for this funding. The authors would also like to acknowledge Candace Halbert, who helped facilitate the Neutron Reflectometry measurements and Ethan Self and Shomaz Ul Haq for help in editing the manuscript. A portion of this research used resources at Spallation Neutron Source an OE Office of Science User Facility operated by the Oak Ridge National Laboratory. The beam time was allocated to the Liquid Reflectometer (LR) on proposal number IPTS-24417. Neutron Depth Profiling measurements were performed at the Nuclear Physics Institute (NPI) in Řež, Czech Republic within the CANAM (Center of Accelerators and Nuclear Analytical Methods) infrastructure at the LVR15 research reactor.

References

1 K. J. Kim, M. Balaish, M. Wadaguchi, L. Kong and J. L. Rupp, Solid-state Li–metal batteries: challenges and horizons of oxide and sulfide solid electrolytes and their interfaces, *Adv. Energy Mater.*, 2021, **11**, 2002689.
2 K. B. Hatzell, *et al.*, Challenges in lithium metal anodes for solid-state batteries, *ACS Energy Lett.*, 2020, **5**, 922–934.
3 K. L. Browning, *et al.*, In Situ Measurement of Buried Electrolyte–Electrode Interfaces for Solid State Batteries with Nanometer Level Precision, *ACS Energy Lett.*, 2023, **8**, 1985–1991.
4 P. Albertus, S. Babinec, S. Litzelman and A. Newman, Status and challenges in enabling the lithium metal electrode for high-energy and low-cost rechargeable batteries, *Nat. Energy*, 2018, **3**, 16–21.

5 P. Albertus, *et al.*, Challenges for and pathways toward Li-metal-based all-solid-state batteries, *ACS Energy Lett.*, 2021, **6**, 1399–1404.
6 T. Famprikis, P. Canepa, J. A. Dawson, M. S. Islam and C. Masquelier, Fundamentals of inorganic solid-state electrolytes for batteries, *Nat. Mater.*, 2019, **18**, 1278–1291.
7 R. Sahore, *et al.*, Practical considerations for testing polymer electrolytes for high-energy solid-state batteries, *ACS Energy Lett.*, 2021, **6**, 2240–2247.
8 A. S. Westover, R. L. Sacci and N. Dudney, Electroanalytical measurement of interphase formation at a Li metal–solid electrolyte interface, *ACS Energy Lett.*, 2020, **5**, 3860–3867.
9 C. Ma, *et al.*, Interfacial stability of Li metal–solid electrolyte elucidated *via in situ* electron microscopy, *Nano Lett.*, 2016, **16**, 7030–7036.
10 G. M. Veith, K. L. Browning, M. Doucet and J. F. Browning, Solid electrolyte interphase architecture determined through *in situ* neutron scattering, *J. Electrochem. Soc.*, 2021, **168**, 060523.
11 T. Fears, *et al.*, Evaluating the solid electrolyte interphase formed on silicon electrodes: a comparison of ex situ X-ray photoelectron spectroscopy and *in situ* neutron reflectometry, *Phys. Chem. Chem. Phys.*, 2016, **18**, 13927–13940.
12 F. Han, *et al.*, High electronic conductivity as the origin of lithium dendrite formation within solid electrolytes, *Nat. Energy*, 2019, **4**, 187–196.
13 K. L. BrowningM. DoucetJ. F. BrowningR. L. Sacci and G. M. Veithin, *Electrochemical Society Meeting Abstracts*, The Electrochemical Society, Inc.2019, vol. 235, p. 526.
14 E. Moyassari, *et al.*, Impact of silicon content within silicon-graphite anodes on performance and Li concentration profiles of Li-ion cells using neutron depth profiling, *J. Electrochem. Soc.*, 2021, **168**, 020519.
15 F. Linsenmann, *et al.*, A liquid electrolyte-based lithium-ion battery cell design for operando neutron depth profiling, *J. Electrochem. Soc.*, 2020, **167**, 100554.
16 J. Jakubek, S. Pospisil, J. Vacik and D. Vavrikin *2012 IEEE Nuclear Science Symposium and Medical Imaging Conference Record*, IEEE, NSS/MIC, 2012, pp. 226–229.
17 G. Ceccio, *et al.*, Study of thin film composites based on LiCoO2 and C60 using neutron depth profiling and atomic force microscopy, *J. Radioanal. Nucl. Chem.*, 2024, **333**, 6687–6697.
18 R. Gilles, How neutrons facilitate research into gas turbines and batteries from development to engineering applications, *J. Surf. Invest.: X-Ray, Synchrotron Neutron Tech.*, 2020, **14**, S69–S74.
19 I. Tomandl, *et al.*, Analysis of Li distribution in ultrathin all-solid-state Li-ion battery (ASSLiB) by neutron depth profiling (NDP), *Radiat. Eff. Defects Solids*, 2020, **175**, 394–405.
20 C. Wang, *et al.*, In situ neutron depth profiling of lithium metal–garnet interfaces for solid state batteries, *J. Am. Chem. Soc.*, 2017, **139**, 14257–14264.
21 M. Trunk, *et al.*, Materials science applications of neutron depth profiling at the PGAA facility of Heinz Maier-Leibnitz Zentrum, *Mater. Charact.*, 2018, **146**, 127–134.
22 M. Avdeev, *et al.*, Monitoring of lithium plating by neutron reflectometry, *Appl. Surf. Sci.*, 2017, **424**, 378–382.
23 M. Avdeev, *et al.*, On nanoscale structure of planar electrochemical interfaces metal/liquid lithium ion electrolyte by neutron reflectometry, *Appl. Surf. Sci.*, 2019, **486**, 287–291.
24 J. Rizell, *et al.*, Neutron Reflectometry Study of Solid Electrolyte Interphase Formation in Highly Concentrated Electrolytes, *Small Struct.*, 2023, **4**, 2300119.
25 D. Cao, Y. Zhang, T. Ji and H. Zhu, In operando neutron imaging characterizations of all-solid-state batteries, *MRS Bull.*, 2023, **48**, 1257–1268.
26 R. F. Ziesche, N. Kardjilov, W. Kockelmann, D. J. Brett and P. R. Shearing, Neutron imaging of lithium batteries, *Joule*, 2022, **6**, 35–52.
27 V. Zinth, *et al.*, Neutron tomography and radiography on a sodium metal halide cell under operating conditions, *J. Electrochem. Soc.*, 2016, **163**, A838.
28 B. Neudecker, N. Dudney and J. Bates, "Lithium-Free" thin-film battery with *in situ* plated Li anode, *J. Electrochem. Soc.*, 2000, **147**, 517.
29 J. Li, C. Ma, M. Chi, C. Liang and N. J. Dudney, Solid electrolyte: the key for high-voltage lithium batteries, *Adv. Energy Mater.*, 2015, **5**, 1401408.
30 N. J. Dudney, Solid-state thin-film rechargeable batteries, *Mater. Sci. Eng., B*, 2005, **116**, 245–249.
31 J. Bates, N. Dudney, B. Neudecker, A. Ueda and C. Evans, Thin-film lithium and lithium-ion batteries, *Solid State Ionics*, 2000, **135**, 33–45.
32 Z. D. Hood, *et al.*, Elucidating interfacial stability between lithium metal anode and Li phosphorus oxynitride *via in situ* electron microscopy, *Nano Lett.*, 2020, **21**, 151–157.
33 D. Cheng, *et al.*, Unveiling the stable nature of the solid electrolyte interphase between lithium metal and LiPON *via* cryogenic electron microscopy, *Joule*, 2020, **4**, 2484–2500.
34 R. Downing, G. Lamaze, J. Langland and S. Hwang, Neutron depth profiling: overview and description of NIST facilities, *J. Res. Natl. Inst. Stand. Technol.*, 1993, **98**, 109.
35 G. P. Lamaze, *et al.*, Cold neutron depth profiling of lithium-ion battery materials, *J. Power Sources*, 2003, **119**, 680–685.
36 X.-L. Zhou and S.-H. Chen, Theoretical foundation of X-ray and neutron reflectometry, *Phys. Rep.*, 1995, **257**, 223–348.
37 A. J. Jackson, *Introduction to Small-Angle Neutron Scattering and Neutron Reflectometry*, NIST Center for Neutron Research, 2008, vol. 1–24.
38 V. Lacivita, *et al.*, Resolving the amorphous structure of lithium phosphorus oxynitride (Lipon), *J. Am. Chem. Soc.*, 2018, **140**, 11029–11038.
39 A. Sacchi, *et al.*, Effect of lithium diffusion into Ga2O3 thin films, *Appl. Surf. Sci.*, 2025, 163974.
40 Z. Warecki, *et al.*, Simultaneous Solid Electrolyte Deposition and Cathode Lithiation for Thin Film Batteries and Lithium Iontronic Devices, *ACS Energy Lett.*, 2024, **9**, 2065–2074.
41 D.-S. Ko, *et al.*, Mechanism of stable lithium plating and stripping in a metal-interlayer-inserted anode-less solid-state lithium metal battery, *Nat. Commun.*, 2025, **16**, 1066.

42 C. Haslam and J. Sakamoto, Stable lithium plating in "lithium metal-free" solid-state batteries enabled by seeded lithium nucleation, *J. Electrochem. Soc.*, 2023, **170**, 040524.
43 I. Pivarníková, *et al.*, Observation of preferential sputtering of Si/graphite anodes from Li-ion cells by GD-OES and its validation by neutron depth profiling, *J. Power Sources*, 2024, **594**, 233972.
44 G. Yang, *et al.*, *Tracking the Initial Capacity Loss in Solid-State Batteries Using In-Situ Neutron Tomography and Raman Imaging*, (2023).
45 K. Kataoka, H. Nagata and J. Akimoto, Lithium-ion conducting oxide single crystal as solid electrolyte for advanced lithium battery application, *Sci. Rep.*, 2018, **8**, 9965.
46 S. Wenzel, S. J. Sedlmaier, C. Dietrich, W. G. Zeier and J. Janek, Interfacial reactivity and interphase growth of argyrodite solid electrolytes at lithium metal electrodes, *Solid State Ionics*, 2018, **318**, 102–112.
47 M. Klenk, *et al.*, Comparative Analysis of Reactivity of Al and Ga Doped Garnet Solid State Electrolyte at the Interface with Li Metal, *ACS Mater. Lett.*, 2024, **6**, 5216–5221.